

## Investigation of the motion of a viscous fluid in the vitreous cavity induced by eye rotations and implications for drug delivery

This article has been downloaded from IOPscience. Please scroll down to see the full text article.

2013 Phys. Med. Biol. 58 1969

(<http://iopscience.iop.org/0031-9155/58/6/1969>)

View [the table of contents for this issue](#), or go to the [journal homepage](#) for more

Download details:

IP Address: 130.251.56.128

The article was downloaded on 12/03/2013 at 11:19

Please note that [terms and conditions apply](#).

# Investigation of the motion of a viscous fluid in the vitreous cavity induced by eye rotations and implications for drug delivery

Andrea Bonfiglio<sup>1</sup>, Rodolfo Repetto<sup>1,2</sup>, Jennifer H Siggers<sup>3</sup>  
and Alessandro Stocchino<sup>1,2,4</sup>

<sup>1</sup> Department of Civil, Chemical and Environmental Engineering, University of Genoa, Genoa, Italy

<sup>2</sup> Center for Material Science and Technology, University of Genoa, Genoa, Italy

<sup>3</sup> Department of Bioengineering, Imperial College London, London, UK

E-mail: [alessandro.stocchino@unige.it](mailto:alessandro.stocchino@unige.it)

Received 25 October 2012, in final form 22 January 2013

Published 4 March 2013

Online at [stacks.iop.org/PMB/58/1969](http://stacks.iop.org/PMB/58/1969)

## Abstract

Intravitreal drug delivery is a commonly used treatment for several retinal diseases. The objective of this research is to characterize and quantify the role of the vitreous humor motion, induced by saccadic movements, on drug transport processes in the vitreous chamber. A Perspex model of the human vitreous chamber was created, and filled with a purely viscous fluid, representing eyes with a liquefied vitreous humor or those containing viscous tamponade fluids. Periodic movements were applied to the model and the resulting three-dimensional (3D) flow fields were measured. Drug delivery within the vitreous chamber was investigated by calculating particle trajectories using integration over time of the experimental velocity fields. The motion of the vitreous humor generated by saccadic eye movements is intrinsically 3D. Advective mass transport largely overcomes molecular diffusive transport and is significantly anisotropic, leading to a much faster drug dispersion than in the case of stationary vitreous humor. Disregarding the effects of vitreous humor motion due to eye movements when predicting the efficiency of drug delivery treatments leads to significant underestimation of the drug transport coefficients, and this, in turn, will lead to significantly erroneous predictions of the concentration levels on the retina.

(Some figures may appear in colour only in the online journal)

<sup>4</sup> Author to whom any correspondence should be addressed.

## 1. Introduction

The vitreous humor is a gel with complex inhomogeneous and viscoelastic rheological properties (Lee *et al* 1992). In this paper, we study fluid motion in the vitreous cavity induced by eye rotations and focus on its effect on intravitreal drug transport. Lund-Andersen (2003) states the generally accepted view that ‘Basically, substances may move by two different processes: diffusion or bulk flow’, and he uses the term ‘bulk flow’ which means that ‘the flow of liquid that enters the vitreous body from the retrozonular space and leaves through the retina . . .’ However, this view neglects advective mass transport due to the flow induced by saccades (that are fast eye rotations performed when redirecting the visual axis to a new location), which might be significant. Indeed, advection due to this flow could explain the dramatic difference observed by Moldow *et al* (1998) between fluorescein transport in gel vitreous humor and liquefied vitreous humor (the latter was observed to have significantly faster mass transport). This flow has also been shown to play an important role in mixing (Stocchino *et al* 2010, Balachandran and Barocas 2011).

Intravitreal drug injection is regularly used to deliver drugs to the retina; see, for example, the reviews by Rittenhouse and Pollack (2000) and Yasukawa *et al* (2004). Pathologies such as cytomegalovirus retinitis, uveitis, proliferative vitreoretinopathy and choroidal neovascularization are often treated with drug delivery systems (Geroski and Edelhauser 2000, Yasukawa *et al* 2004). Intravitreal drug delivery has several advantages over systemic delivery because it bypasses the blood-retinal barrier (Cunha-Vaz 2004), thus allowing the drug to reach the retina in high concentrations. The concentration of the drug at the retina after injection depends on transport processes within the vitreous humor. When the vitreous humor is in the gel state, drug transport is not affected significantly by the rheology of the vitreous humor, but, once the gel structure degenerates and liquefaction occurs, advective transport induced by eye rotations dwarfs the contribution of diffusion to transport, and, in this case, the rheology of the vitreous is significant. It is therefore important to understand how the rheology of the vitreous humor, and particularly its viscosity, affects advective transport in the vitreous chamber, and this is a main aim of this paper. It has also been suggested that the higher mass transport capability of vitreous humor replacement fluids that are used after vitrectomy leads to an increased oxygen concentration at the retina, which is thought to be responsible for the increased incidence of cataract in these patients (Holekamp 2010).

In order to quantify and predict the efficiency of drug delivery, it is essential to understand mass transport processes occurring in the vitreous humor; therefore, several researchers have made *in vivo* measurements of concentration of solutes in the vitreous humor (López-Cortés *et al* 2001, Kim *et al* 2004, Anand *et al* 2004). Comprehensive reviews of transport phenomena in the eye from the biomechanical point of view are given by Ethier and Simmons (2007) and Siggers and Ethier (2012). An extensive literature on purely diffusive drug transport in the vitreous chamber exists, based on theoretical/numerical models (Friedrich *et al* 1997a, 1997b, Tojo and Isowaki 2001, Ranta and Urtti 2006). The bulk flow within the vitreous humor due to a pressure gradient from the anterior of the eye to the posterior pole has been studied by various authors (Stay *et al* 2003, Kathawate and Acharya 2008). Advective mass transport induced by vitreous humor also plays an important role in intravitreal drug delivery, and an improved understanding of flow and advection is vital to inform this procedure better. Unfortunately, there are only relatively few *in vivo* measurements of flow of the vitreous humor available in the literature (Walton *et al* 2002, Piccirelli *et al* 2012, Rossi *et al* 2012), and further studies in this field would be necessary to obtain a more detailed description of motion of the vitreous humor. Using *in vitro* experiments, Repetto *et al* (2008) studied the flow generated in the vitreous chamber by saccades, and commented on the implications for mass

transport processes. They considered a simple spherical experimental model of the eye, used a viscous fluid to mimic the vitreous humor and studied the flow generated by periodic sinusoidal torsional rotations of the domain about a fixed axis through the center of the sphere. Although the flow is predominantly sinusoidally oscillating, a small steady component also exists that can be calculated analytically. This component plays a major role in mass transport processes; see also section 3.4. Stocchino *et al* (2010) also studied mixing processes associated with the steady component of the flow, but considered a more realistic shape of the vitreous chamber, which included an indentation in the anterior part reproducing the presence of the lens. The authors measured the steady component of the flow on the plane of symmetry orthogonal to the axis of rotation. They showed that flow characteristics are very complex, and several vortices exist that organize the plane into regions with different mixing properties. Mass transport properties are therefore, correspondingly, qualitatively different within these regions (Oliveri *et al* 2011). Repetto *et al* (2010) and Balachandran and Barocas (2011) studied analytically and numerically the effect of eye rotations on mass transport processes within the vitreous chamber, and calculated that advective transport is much faster than diffusive transport. Balachandran and Barocas (2011) also studied how transport processes in the vitreous humor affect drug outflow from different pathways.

In this paper, we obtain a more detailed and, crucially, three-dimensional (3D) understanding of the saccade-induced steady component of the flow in the vitreous humor than in previous works. We use a quasi-spherical model of the eye that includes an indentation representing the lens, and investigate the flow due to periodic, sinusoidal rotations about a fixed axis. We model the vitreous humor as a purely viscous fluid, thus neglecting viscoelastic effects. We measure the steady component of the flow on many planes orthogonal to the axis of rotation and use a mathematical technique to reconstruct the 3D velocity field. We then compute 3D particle trajectories and investigate how a drug inserted at a given position in the vitreous chamber would disperse in time.

## 2. Material and methods

### 2.1. *In vitro* model of the vitreous chamber

We perform experiments on a magnified scale model of the vitreous chamber, using an experimental apparatus based on that described by Repetto *et al* (2005), suitably modified to allow measurements to be acquired on different planes perpendicular to the axis of rotation. We use a plexiglas cylinder with an internal cavity. Since the lens is by far the most prominent non-spherical feature of the vitreous chamber, we focus on its effect, neglecting additional geometrical features, similarly to the studies of Stocchino *et al* (2010), Balachandran and Barocas (2011) and Repetto *et al* (2010), and make the cavity to be a sphere of radius  $R = 4.08$  cm with an indentation of depth  $L$  (see figure 1). *In vivo* measurements indicate that the ratio  $L/R$  displays a large amount of inter-subject and intra-subject variations (the intra-subject variation is caused by the lens focusing on different distances). For the present experimental study, we use a model of the vitreous cavity with an indentation of depth equal to  $0.3R$ . The model is filled with aqueous solutions of glycerol at different concentrations. The resulting mixture has Newtonian properties (i.e. it is a purely viscous fluid); therefore, we neglect the viscoelastic behavior of the vitreous humor as well as its inhomogeneities. For this reason, our results are most relevant to represent the behavior of tamponade fluids or extensively liquefied vitreous humor.

The model is mounted on a support connected to a computer-controlled motor that can induce rotations of the container with any prescribed time dependence. For simplicity, we only

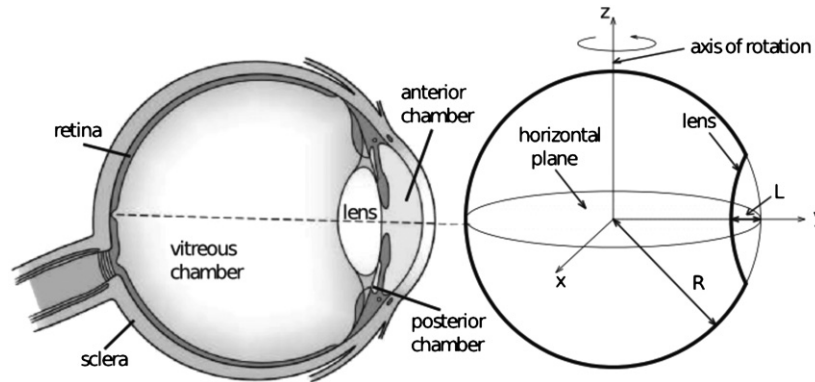


**Figure 1.** Sketch of the sagittal section of the eye (left) and of the experimental model, with a notation (right).

consider purely sinusoidal rotations, i.e.  $\varepsilon(t) = A \sin(\omega t)$ , where  $\varepsilon$  is the angular displacement,  $t$  is the time,  $A$  is the amplitude of eye rotations and  $\omega$  their angular frequency. Becker (1989) reports that the relationship between saccade duration  $D$  and saccade amplitude  $A$  is well described by the following linear relationship:

$$D = D_0 + dA \quad (1)$$

valid in the range  $5^\circ < A < 50^\circ$ , and with  $d \approx 0.0025 \text{ s deg}^{-1}$  and  $0.02 \leq D_0 \leq 0.03 \text{ s}$ . Becker (1989) also suggests that the ratio  $\Omega_p/\bar{\Omega}$  between the peak angular velocity of the eye bulb  $\Omega_p$  and its average value  $\bar{\Omega} = A/D$  is approximately constant and equal to 1.64. In this work, we consider small amplitude eye rotations, with  $A = 5^\circ$ , and, following Balachandran and Barocas (2011), define the angular frequency of the periodic rotations as  $\omega = 2\pi f = 2\pi/2D$ , with  $D$  computed from equation (1). Therefore, we assume a sequence of consecutive eye rotations with the opposite direction, amplitude  $A = 5^\circ$  and duration  $D$  equal to 0.0375 s. Obviously, since a single saccadic eye rotation is not sinusoidal (i.e. it does not precisely fit half of a sine function), the relationship  $\Omega_p/\bar{\Omega} \approx 1.64$  does not hold for the rotations we impose.

A summary of the experimental parameters is given in table 1, where for each experiment, we have indicated the value of the oscillation frequency  $f$ , the density  $\rho$ , the dynamic viscosity  $\mu$ , the kinematic viscosity  $\nu$  of the fluid and the corresponding Womersley number  $\alpha$ , defined in the next section.

As discussed by Repetto *et al* (2010), the motion of a viscous fluid induced within a given domain by sinusoidal rotations of the container is governed by two dimensionless parameters: the Womersley number, defined as  $\alpha = R\sqrt{\omega/\nu}$  with  $\nu$  being the kinematic viscosity, and the oscillation amplitude  $A$ . The Womersley number can be interpreted as the square root of the ratio of the timescale of viscous transport of momentum across the sphere to the timescale of rotations. Since we use a magnified model of the vitreous chamber, scale effects need to be correctly accounted for. In order to ensure similitude between the model and the prototype (i.e. the real eye), we need to preserve both dimensionless parameters and use geometric similarity for the domain shape.

In the present experiments, as discussed above, we choose to fix the angular frequency of oscillations ( $\omega = 2\pi/2D \approx 84 \text{ rad s}^{-1}$ ). Moreover, we consider a fixed size of the eye ( $R = 1.2 \text{ cm}$ ). Therefore, changes in the Womersley number are only related to changes of vitreous humor viscosity. The kinematic viscosity  $\nu$  of the vitreous humor can assume values

**Table 1.** Main experimental parameters (relative to the model). For all experiments, the oscillation amplitude  $A$  has been set equal to  $5^\circ$ .

Experiment number	$f$ (Hz)	$\rho$ (Kg dm <sup>-3</sup> )	$\mu$ (Pa s)	$\nu$ (m <sup>2</sup> s <sup>-1</sup> )	$\alpha$
1	1	1.259	0.837	$6.7 \times 10^{-4}$	3.9
2	2	1.259	0.837	$6.7 \times 10^{-4}$	5.6
3	3	1.259	0.837	$6.7 \times 10^{-4}$	6.9
4	4	1.259	0.837	$6.7 \times 10^{-4}$	7.9
5	5	1.259	0.837	$6.7 \times 10^{-4}$	8.8
6	6	1.259	0.837	$6.7 \times 10^{-4}$	9.7
7	7	1.259	0.837	$6.7 \times 10^{-4}$	10.5
8	8	1.259	0.837	$6.7 \times 10^{-4}$	11.2
9	9	1.259	0.837	$6.7 \times 10^{-4}$	11.9
10	10	1.259	0.837	$6.7 \times 10^{-4}$	12.5
11	1	1.215	0.0535	$4 \times 10^{-5}$	15.4
12	2	1.215	0.0535	$4 \times 10^{-5}$	21.8
13	3	1.215	0.0535	$4 \times 10^{-5}$	26.7
14	4	1.215	0.0535	$4 \times 10^{-5}$	30.8
15	5	1.215	0.0535	$4 \times 10^{-5}$	34.5
16	6	1.215	0.0535	$4 \times 10^{-5}$	37.7
17	7	1.215	0.0535	$4 \times 10^{-5}$	40.8
18	8	1.215	0.0535	$4 \times 10^{-5}$	43.6
19	9	1.215	0.0535	$4 \times 10^{-5}$	46.2
20	10	1.215	0.0535	$4 \times 10^{-5}$	48.7

within a very wide range, from approximately  $\nu \approx 10^{-6} \text{ m}^2 \text{ s}^{-1}$  (viscosity of water), in the case of extensively liquefied vitreous humor, up to  $\approx 5 \times 10^{-3} \text{ m}^2 \text{ s}^{-1}$ , in the case of highly viscous tamponade fluids. This implies that  $\alpha$  is able to vary from  $\approx 1.5$  to  $\approx 110$ . As shown in table 1, owing to limitations of the experimental apparatus, we considered a smaller range ( $3.9 \leq \alpha \leq 48.7$ ), which corresponds to values of the viscosity at the prototype scale between  $\approx 5 \times 10^{-6} \text{ m}^2 \text{ s}^{-1}$  (largest value of  $\alpha$ ) and  $\approx 8 \times 10^{-4} \text{ m}^2 \text{ s}^{-1}$  (lowest value of  $\alpha$ ), which spans a range of cases of clinical interest.

## 2.2. Experimental procedure and data analysis

When the eye model undergoes periodic rotations, the largest component of the resulting flow in the fluid is the component that oscillates with the same frequency as the rotations, which we refer to as the primary flow. The primary flow causes the majority of the wall shear stress, which is important because of its possible connection to the generation of retinal detachment. The primary flow was studied using an *in vitro* setup similar to that presented here and using a purely viscous Newtonian fluid by Repetto *et al* (2005), in the case of a spherical domain, and by Stocchino *et al* (2007), who also accounted for the indentation produced by the lens.

Despite the fact that the forcing flow is periodic, a steady component of the flow is also generated, which is called steady streaming, and is known to occur in several fluid mechanical systems. Although the magnitude of the steady streaming is usually much smaller than that of the primary flow, this component is important because it makes a dominant contribution to mass (drug) transport. This is because it induces a net particle drift over a cycle, unlike the primary flow, which induces a much smaller net drift than the velocities involved, due to cancellation over the cycle. In this paper, we focus on the steady component of the flow.

Using Cartesian coordinates  $(x, y, z)$  with an origin at the center of the model and with  $z$  coincident with the axis of rotation, we took images on the planes  $z = (\text{constant})$  (horizontal

plane) measuring the  $x$  and  $y$  velocity components or on the symmetry plane  $x = 0$  (vertical plane), measuring the  $y$  and  $z$  velocity components (see figure 1).

In each experiment, we took measurements of the steady streaming velocity on 39 horizontal planes, corresponding to different values of  $z$ , using the particle image velocimetry (PIV) technique. In order to directly measure the steady streaming, we analyzed couples of images separated in time by a multiple of the oscillation period (in a range from 1 to 5, depending on the maximum velocity). This allowed us to measure the displacement field of particles after an integer number of cycles. In this way, we obtained the  $x$  and  $y$  components of the steady streaming flow  $u(x, y, z)$  and  $v(x, y, z)$ , on each of these planes (see figure 1).

In this study, we used an Nd-Yag laser, with a pulse duration of 60 ns, and hollow glass spheres with a mean diameter of 5  $\mu\text{m}$  as tracer particles. For the PIV analysis of the images, we used the commercially available software IDT Provision. From each couple of images, a velocity vector field was obtained, with a spatial resolution such that approximately 50 velocity vectors along the diameter of the equatorial plane were determined. For every run, we acquired 100 images on each  $z$ -plane, and obtained the corresponding flow fields. These were averaged to extract a mean ( $x - y$ ) two-dimensional (2D) velocity field for each  $z$ -plane.

In order to reconstruct the third velocity component  $w(x, y, z)$ , we used a technique, based on applying mass conservation. For an incompressible fluid (i.e. a fluid with constant density), the flow satisfies the continuity equation:

$$\frac{\partial w}{\partial z} = -\frac{\partial u}{\partial x} - \frac{\partial v}{\partial y} \quad (2)$$

(it is possible to show that this equation also holds for the steady component of the flow). The right-hand side of the above equation is known from the experimental measurements on each plane. Therefore, in order to evaluate the third component of the flow,  $w$  would suffice to integrate the above equation with respect to  $z$ , starting from a plane where  $w$  is known, for instance the equatorial plane  $z = 0$ , on which the (assumed) symmetry of the flow imposes the condition  $w = 0$ . However, as a consequence of experimental inaccuracy and/or insufficient spatial resolution, we found that the direct integration of the continuity equation did not lead to satisfactory results since significant fluxes through the domain boundary were often predicted. This cannot be avoided with this method since a first-order differential equation is solved and therefore only one boundary condition can be imposed. For this reason, we have used a different method. Instead of enforcing the continuity equation to be satisfied exactly, we seek values of the third component of the velocity that satisfy the no-slip condition exactly and that minimize the average inaccuracy in the continuity equation (2). Specifically, we minimize the average value of  $(\nabla \cdot \mathbf{u})^2 = (\partial u/\partial x + \partial v/\partial y + \partial w/\partial z)^2$  over the whole domain, which leads to the following equation for  $w$ :

$$\frac{\partial^2 w}{\partial z^2} = -\frac{\partial}{\partial z} \left( \frac{\partial u}{\partial x} + \frac{\partial v}{\partial y} \right). \quad (3)$$

The right-hand side can be estimated from measurements, allowing us to calculate, for each value of  $x$  and  $y$ , the  $z$  velocity component  $w$ , imposing the following two boundary conditions:  $w = 0$  at  $z = 0$  and  $w = 0$  at the wall. Equation (3) was solved using a finite-difference second-order implicit scheme. This approach leads to similar results as the direct integration of the continuity equation in the core of the domain and performs more satisfactorily close to the boundary.

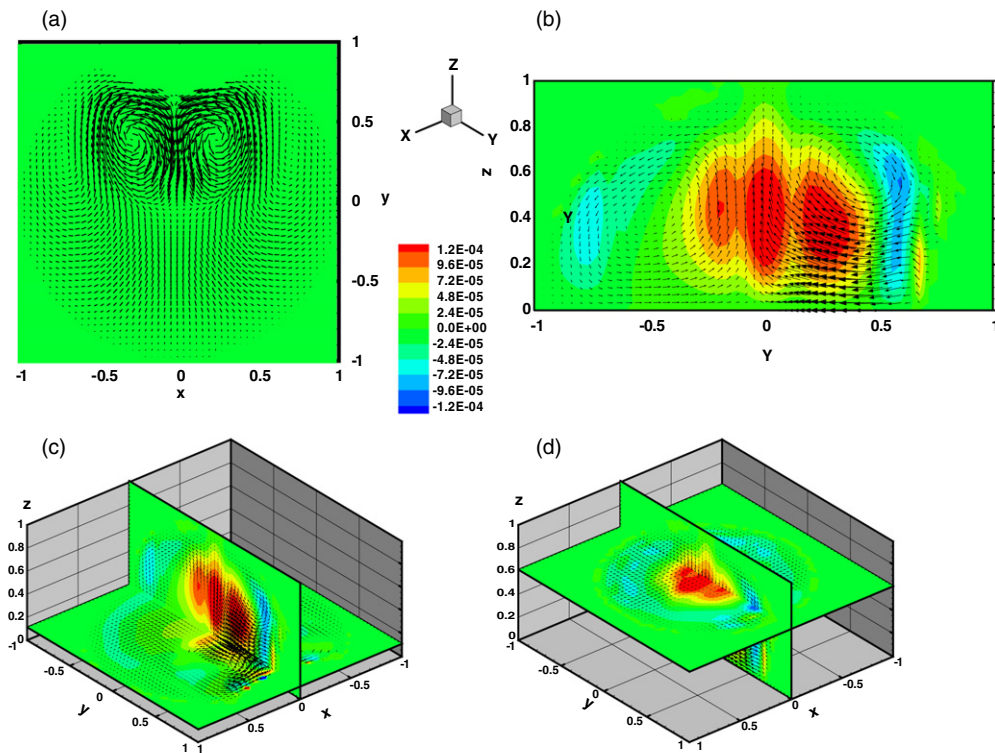


**Figure 2.** Cross-sections of the reconstructed 3D steady streaming flow field  $\mathbf{u}$ , for  $\alpha = 5.6$  and  $A = 5^\circ$ : (a)  $z = 0$ , (b)  $x = 0$ ; (c)  $z = 0.1R$  and  $x = 0$ ; (d)  $z = 0.6R$  and  $x = 0$ . The velocity is scaled with  $\omega R$  (experiment 2).

### 3. Results

#### 3.1. Vitreous motion

In figures 2 and 3, we show various cross-sections of the reconstructed steady streaming flow, for two different values of the Womersley number. The arrows show the steady streaming velocity vectors and the colors represent the intensity of the  $z$ -component of the velocity,  $w$ , obtained from the solution of equation (3).

Measurements show that the structure of the flow is very complex. At the back of the vitreous chamber, the flow is quite similar to that observed in a perfect sphere (Repetto *et al* 2008): particles close to the equatorial plane orthogonal to the axis of rotation ( $z = 0$ ) move toward the center of the domain, then toward the poles along the  $z$ -axis and back again along the curved walls toward the plane  $z = 0$ . However, the flow in the anterior segment of the vitreous chamber model is significantly affected by the presence of the lens. This was also found to be the case for the primary oscillatory flow (Stocchino *et al* 2007, Repetto *et al* 2010, Balachandran and Barocas 2011).

For small values of the Womersley number, i.e. very viscous vitreous humor (figure 2), two circulation cells are generated on the equatorial plane, which are reflections of one another in the plane of symmetry,  $x = 0$ , (see figure 2(a)). Within these circulations, fluid flows from the apex of the lens toward the center of the domain. Figure 2(c) shows the velocity field on

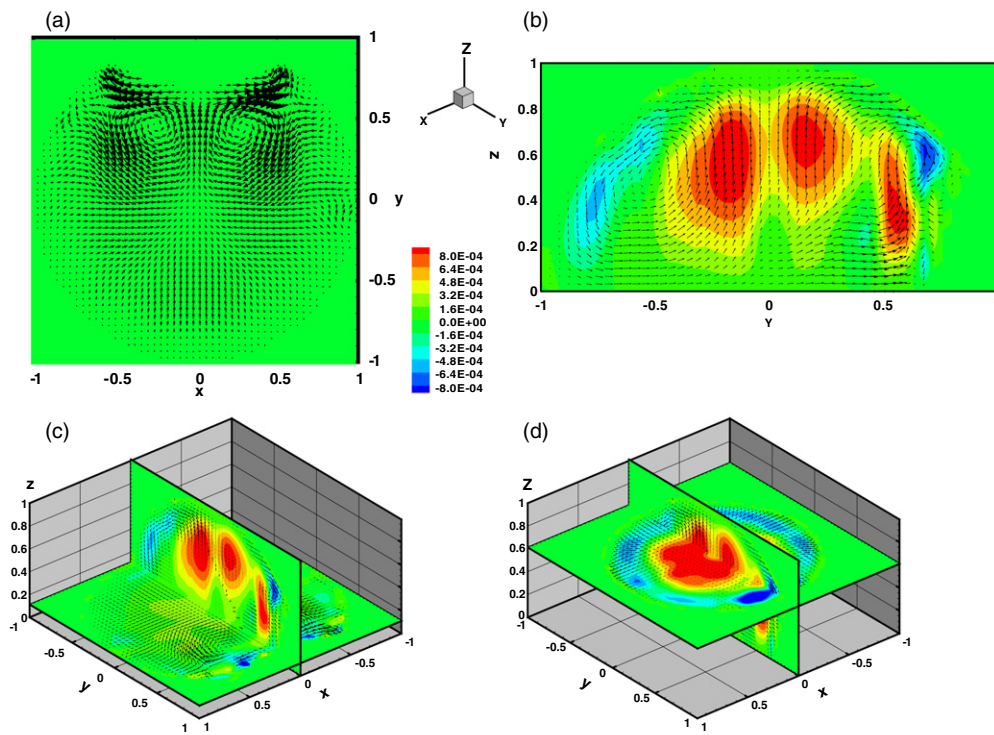
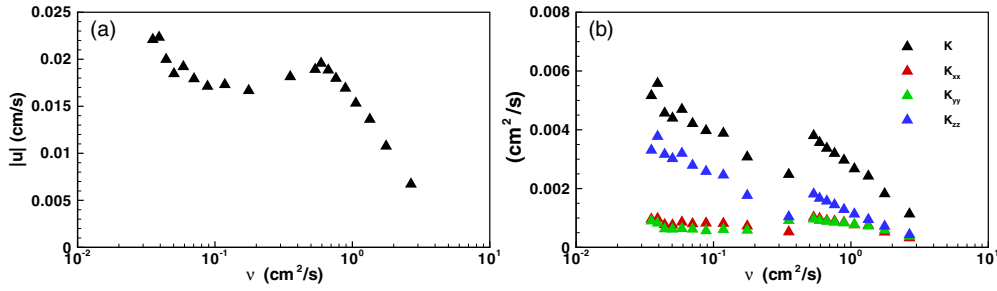


Figure 3. Same as in figure 2 but with  $\alpha = 46.2$  (experiment 19).

the plane  $z = 0.1R$  and demonstrates that the circulation cells extend in the  $z$ -direction. The centers of the two circulations get closer to one another as  $z$  increases, and for  $z \approx 0.6R$ , the circulation cells disappear; see figure 2(d). For larger values of the Womersley number, reported in figure 3, the steady streaming flow is qualitatively very different, and it is dominated by two new circulation cells that rotate in the opposite sense with respect to those shown in figure 2. Thus, our experiments predict that when vitreous humor viscosity is small (large values of  $\alpha$ ), fluid particles are rapidly swept all the way from the back to the front of the vitreous chamber model. This is expected to have important implications for the transport of drugs, as in this case there is a much faster connection between anterior and posterior segments of the vitreous chamber.

In figure 4(a), we show the dependence of the steady streaming intensity  $U$  at the prototype scale, defined as the spatial average of the velocity magnitude over the whole domain, versus vitreous viscosity  $\nu$ . The streaming intensity generally decreases with increasing  $\nu$ , particularly at large values of the viscosity, as expected. However, the decrease of  $U$  is not monotonic and a relative minimum is found for  $\nu \approx 0.2 \text{ cm}^2 \text{ s}^{-1}$ . This behavior is similar to the one described by Stocchino *et al* (2010) on the basis of 2D measurements. However, we stress that the plot is now based on a volume average of the fully 3D flow field. The non-monotonic decrease of the steady streaming intensity for increasing values of the vitreous humor viscosity can be attributed to changes of the characteristics of the two circulation structures forming close to the lens that with decreasing  $\nu$  (growing  $\alpha$ ) modify their sense or rotation, and have small intensity for the values of  $\nu$  (or  $\alpha$ ) corresponding to the transition from one sense to another. We note that the magnitude of the average velocity ranges between  $6 \times 10^{-3}$  and



**Figure 4.** (a) Intensity of the steady streaming  $U$  against vitreous viscosity  $\nu$ .  $U$  is defined as the spatial average of the velocity magnitude over the volume of the domain. (b) Behavior of the total dispersion coefficient as a function of the viscosity; the values are rescaled to real conditions.

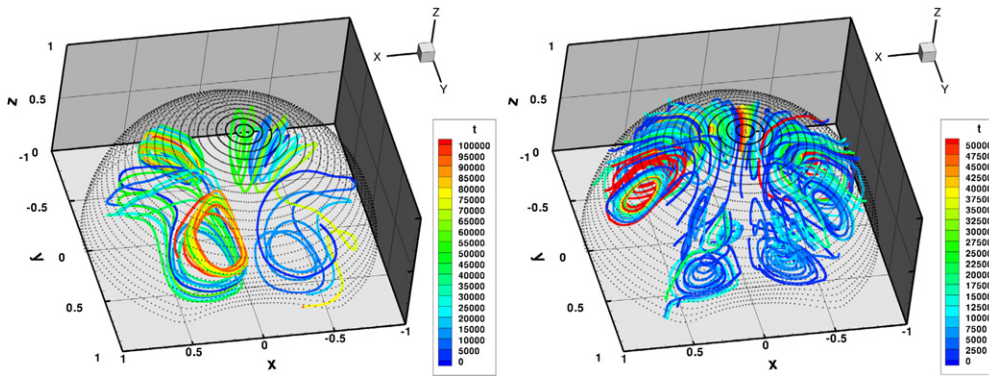


**Figure 5.** Examples of computed trajectories of particles released from various points in the vitreous chamber in the same experiments as shown in figures 2 and 3. The colors show the time of integration (in numbers of periods of oscillation).

$2.2 \times 10^{-2} \text{ cm s}^{-1}$ , meaning that the timescale required for a particle to run the distance corresponding to the characteristic size of the domain ( $R = 1.2 \text{ cm}$ ) is of the order of minutes. Assuming a diffusion coefficient in the vitreous  $D_{\text{diff}} = 5 \times 10^{-6} \text{ cm}^2 \text{ s}^{-1}$  (Stay *et al* 2003) and using  $R$  as the length scale, we estimate values of the Péclet number  $Pe = UR/D$  ranging between 1440 and 5280. This shows that advection significantly dominates over diffusion.

### 3.2. Particle trajectories

In order to obtain a better understanding of the flow-field 3D structure, we compute particle trajectories. We note that if diffusion processes are neglected, a drug particle in the fluid would move exactly along a fluid particle trajectory. In figure 5, we report particle trajectories relative to 50 000 cycles of oscillation, which corresponds to a time of approximately 1 h ( $2\pi \times 50\,000/\omega$ ). Since eye rotations are not periodic and periods of rest occur between sequences of rotations, we should consider a somewhat longer duration than the reality, albeit of the same order of magnitude. On the timescale  $T$  of 1 h, and with a diffusion coefficient  $D_{\text{diff}} = 5 \times 10^{-6} \text{ cm}^2 \text{ s}^{-1}$ , the characteristic diffusion length  $\delta$  is equal to  $\delta \approx \sqrt{TD_{\text{diff}}} \approx 1 \text{ mm}$ , which is quite small compared to the size of the vitreous chamber ( $\approx 1 \text{ cm}$ ). This implies that

over times smaller than  $\approx 1$  h and for the eye rotations considered here, particle trajectories are good approximations of paths followed by drug particles within the vitreous chamber.

The determination of particle trajectories corresponding to a velocity field is also important since knowledge of particle paths represents the basis for studying dispersion processes that will be addressed in the next section.

Particle trajectories for the cases of  $\alpha = 5.6$  and  $\alpha = 46.2$  are shown in figure 5. The color along each curve indicates the time progression, from blue to red. Fluid particles at the back of the vitreous chamber model move along approximately helical paths, mainly moving along vertical planes. On the other hand, trajectories in the anterior part of the vitreous chamber are strongly influenced by the presence of the circulation cells close to the lens and particles in that region remain trapped for long times in the circulation structures. At low values of the Womersley number, particle trajectories are quite regular, whereas they appear to be more complex (and irregular, also possibly as a consequence of larger experimental errors) at higher values of  $\alpha$ . In all cases, this visualization of the flow clearly shows that the flow is highly 3D and the  $z$ -component of the steady streaming velocity is comparable to the  $x$ - and  $y$ -components, implying that, as a consequence of the closeness of the domain and of its particular shape, rotations about a fixed axis generate a velocity field in which all three (steady streaming) velocity components have the same order of importance.

### 3.3. Drug dispersion coefficients

Starting from particle trajectories, we perform an analysis of the Lagrangian mixing processes in the vitreous chamber model, extending to the 3D case the 2D analysis described by Stocchino *et al* (2010). In particular, we compute the dispersion coefficient  $\mathbf{K}$ , which is an average measure (over the whole domain) of the rate of spreading of the particles in the domain, and has the dimensions of the molecular diffusion coefficient  $D_{\text{diff}}$ , i.e. length squared over time (see, for instance, Stocchino *et al* (2010) for a precise mathematical definition). Owing to the complexity of the flow fields described in the previous sections, transport phenomena related to advection are anisotropic, i.e. the dispersion coefficient assumes different values depending on the direction considered. Mathematically, this implies that  $\mathbf{K}$  is a tensorial quantity (i.e. represented by a  $3 \times 3$  symmetric matrix). We evaluate  $K_{xx}$ ,  $K_{yy}$  and  $K_{zz}$ , being the dispersion coefficients along the orthogonal directions  $x$ ,  $y$  and  $z$ , and plot them in figure 4(b) as a function of the viscosity of the vitreous humor. The three values  $K_{xx}$ ,  $K_{yy}$  and  $K_{zz}$  are quite different from one another and the dominant direction of transport is the  $z$ -direction. This means that since eye rotations preferentially occur about a vertical axis, drug transport after an intravitreal injection is, somewhat surprisingly for horizontal saccades, expected to be (at least for relatively short times) more efficient in the vertical direction. In the figure, we also plot the global dispersion coefficient  $K$ , defined as the sum of the three values ( $K = K_{xx} + K_{yy} + K_{zz}$ ). The global dispersion coefficient generally decreases with increasing  $\nu$ , from  $\approx 6 \times 10^{-3} \text{ cm}^2 \text{ s}^{-1}$  to  $\approx 10^{-3} \text{ cm}^2 \text{ s}^{-1}$ , and thus all values are several orders of magnitude larger than that of the molecular diffusion coefficient. This confirms that for all fluids considered, when the vitreous chamber is filled with a purely viscous fluid, advective transport largely dominates over diffusion. The sudden increase of value of the dispersion coefficients at  $\nu \approx 0.5 \text{ cm}^2 \text{ s}^{-1}$  can again be attributed to the qualitative change in the spatial structure of the velocity field.

### 3.4. Intravitreal drug dispersion

In this section, we model the dispersion of a drug inserted at a certain position in the vitreous chamber. To this end, we integrate numerically particle trajectories starting from

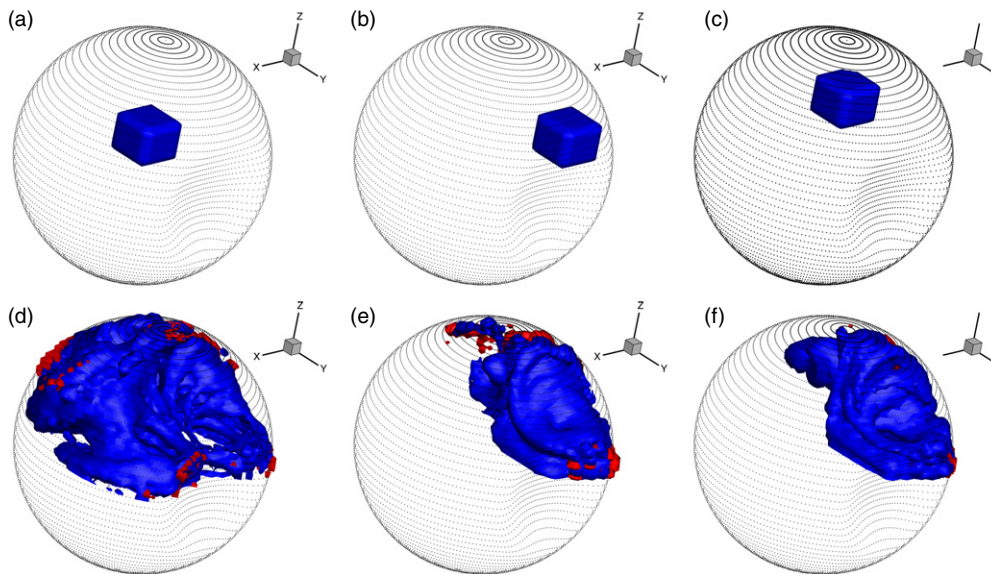


**Figure 6.** Isosurfaces of concentration: (a)–(c), initial time; (d)–(f), final time. Initial location of particles: (a)  $x = 0$ ,  $y = 0$ ,  $z = 0.15 R$ ; (b)  $x = -0.6 R$ ,  $y = 0.3 R$ ,  $z = 0.15 R$ ; (c)  $x = -0.6 R$ ,  $y = -0.45 R$ ,  $z = 0.15 R$ .

the experimental data. We choose a cubic region of side length  $0.31R$  within the eye model and place  $10^6$  labeled particles at random within it, which we follow over time. In order to visualize the dispersion process, we subdivide the domain in a large number of cells ( $\approx 4 \times 10^4$ ) and use the number of labeled particles contained in each cell as a measure of their ‘concentration’, which is thus dependent on time and space. If the number of particles is large enough, this concentration can be thought of as a continuous function of time and space, and we visualize it by plotting its isosurfaces (figure 6). We test three different initial locations, shown in figure 6: (a) close to the center of the domain, (b) in the anterior part of the domain, close to the lens and upper hemisphere and (c) in the posterior part of the domain and upper hemisphere. The initial volume of the bolus of drug in the current work closely resembles the dosage of common intravitreal medications (e.g. bevacizumab, ranibizumab and ganciclovir, among others). In fact, assuming a typical value of the eye radius of 1.2 cm, the drug volume is found to be 0.05 ml (about 0.7% of the vitreous chamber). We assume that drug particles behave exactly as fluid particles, under the assumption of neglecting molecular diffusion, and for this reason, as discussed in the previous section, the results are only valid for relatively short times ( $< 1$  h). However, this initial phase may be relevant as large gradients of drug concentration are expected to occur initially through the retinal layers, and therefore initial absorption rates are probably quite high. In figures 6(d)–(f), we use two different colors to identify regions of the surface in which the labeled particles are moving (blue) from regions in which particles are so close to the wall that they do not move far (red). Note, however, that we do not use an absorption condition at the wall and therefore mass (i.e. the number of labeled particles) is preserved within the domain.

The results confirm that the dispersion process is much more efficient than if only molecular diffusion were considered. In fact, in all cases, at the final time, which corresponds to approximately 1 h of real time, the particles were found to have dispersed throughout a considerable proportion of the domain. The particular spatial structure of the flow field,

however, makes the results quite sensible to the location of particle release. In particular, in case (a), when the particles are inserted around the axis of rotation and very close to the center of the domain, within 1 h particles have spread all over the upper hemisphere of the domain. On the other hand, the dispersion processes in cases (b) and (c) look quite similar, and, after tracking the particles, they are still confined within the half of the upper hemisphere corresponding to negative values of  $x$ . In other words, particles have failed to cross the symmetry plane  $x = 0$ .

#### 4. Discussion

In this paper, we carried out experiments on a magnified scale model of the vitreous chamber and measured the steady component of the flow field occurring as a result of eye rotations. We focused on the steady component of the flow because it contributes dominantly to advection, whereas the oscillatory component induces a much slower net motion. We measured the velocity field on many planes orthogonal to the axis of rotation and reconstructed the third velocity component numerically. Our results confirm that when the vitreous humor is liquefied, transport of drugs in the vitreous humor is largely dominated by advection (advection being several orders of magnitude larger than diffusion). We also show that mass transport is anisotropic in the vitreous chamber, and the transport in the direction of the axis of rotation is more efficient than in the antero-posterior and nasal-temporal directions. We show that the initial dispersion process taking place after a drug injection is significantly affected by the location of the injection because the flow field is characterized by symmetry planes that are not easily crossed by particles, unless the timescales considered are long enough for diffusion to come into play. The relevance of this finding depends on the absorption rate of the drug at the retina, which has not been considered in this work. However, we can anticipate that if the timescale characteristic for drug absorption at the retina is smaller, or comparable to the timescale for drug dispersion throughout the vitreous chamber, then the location of the injection is likely to affect the spatial distribution of drug uptake on the retina significantly. On the other hand, if the uptake of drug on the retina is a slower process, it is reasonable to expect a uniform absorption of the drug. This work allows us to obtain a reliable estimate for the timescale of drug dispersion in the vitreous chamber, which is found to be of the order of hours. The work, therefore, represents a useful step to inform the dose during intravitreal drug release, and also confirms the importance of considering the rheology of the vitreous humor in order to design the intervention appropriately (Stocchino *et al* 2010, Balachandran and Barocas 2011, Repetto *et al* 2010).

The work is based on several simplifying assumptions that are recalled and briefly commented upon in the following. The vitreous has been modeled as a Newtonian homogeneous fluid. For this reason, our results are most relevant to the case of vitrectomized patients, with tamponade fluids or aqueous replacing the vitreous, and also patients whose vitreous is extensively liquefied. Understanding transport phenomena in eyes with tamponade fluids is clinically relevant since it has been suggested that the higher mass transport capacity of such fluids with respect to the vitreous under physiological conditions leads to an increased oxygen concentration at the retina, which is thought to be responsible for the increased incidence of cataract in these patients (Holekamp 2010).

We have only considered periodic sinusoidal rotations of the domain. Real eye rotations are not truly periodic; however, the experiments performed by Repetto *et al* (2005) with purely Newtonian fluids indicate that, starting from rest, the motion is very close to periodic after only a few rotations of the domain (at least for relatively small values of the Womersley number). We modeled the vitreous chamber as a sphere with an indentation in the shape of

a spherical cap and have neglected other geometrical features of the real vitreous chamber shape. We believe that although adding more realistic features of the geometry would add to the complexity of the model, this would not alter dramatically the results obtained, and would not modify qualitatively the main findings of this work.

Summarizing, we have studied mass transport processes in a physical model of the vitreous cavity, focusing on advection induced during rotations of the eyeball. We extended results obtained in our previous contributions, by obtaining a fully 3D description of the flow field and by directly studying the dispersion of particles released in the domain. We believe that this improves our understanding of the fluid dynamics of the vitreous humor. An estimate of the time required for drugs to disperse through the vitreous chamber was obtained and was related to the mechanical characteristics of the vitreous. Our results could also serve as a benchmark to test the validity of numerical simulations employed in the design of intravitreal drug delivery interventions.

It is possible that even in the case of a normal gel vitreous humor, eye rotations could significantly influence drug transport processes in the eye. We are currently performing experiments using a viscoelastic fluid in order to investigate this.

## References

- Anand B S, Atluri H and Mitra A K 2004 Validation of an ocular microdialysis technique in rabbits with permanently implanted vitreous probes: systemic and intravitreal pharmacokinetics of fluorescein *Int. J. Pharm.* **281** 79–88
- Balachandran R K and Barocas V H 2011 Contribution of saccadic motion to intravitreal drug transport: theoretical analysis *Pharm. Res.* **28** 1049–64
- Becker W 1989 *The Neurobiology of Saccadic Eye Movements* ed R H Wurtz and M E Goldberg (New York: Elsevier)
- Cunha-Vaz J G 2004 The blood-retinal barriers system. Basic concepts and clinical evaluation *Exp. Eye Res.* **78** 715–21
- Ethier C R and Simmons C A 2007 *Introductory Biomechanics—From Cells to Organisms (Cambridge Texts in Biomedical Engineering)* (Cambridge: Cambridge University Press)
- Friedrich S, Cheng Y L and Saville B 1997a Drug distribution in the vitreous humor of the human eye: the effects of intravitreal injection position and volume *Curr. Eye Res.* **16** 663–9
- Friedrich S, Cheng Y L and Saville B 1997b Finite element modeling of drug distribution in the vitreous humor of the rabbit eye *Ann. Biomed. Eng.* **25** 303–14
- Geroski D H and Edelhauser H F 2000 Drug delivery for posterior segment eye disease *Invest. Ophthalmol. Vis. Sci.* **41** 961–4
- Holekamp N M 2010 The vitreous gel: more than meets the eye *Am. J. Ophthalmol.* **149** 32–6
- Kathawate J and Acharya S 2008 Computational modeling of intravitreal drug delivery in the vitreous chamber with different vitreous substitutes *Int. J. Heat Mass Transfer* **51** 5598–609
- Kim H, Robinson M R, Lizak M J, Tansey G, Lutz R J, Yuan P, Wang N S and Csaky K G 2004 Controlled drug release from an ocular implant: an evaluation using dynamic three-dimensional magnetic resonance imaging *Invest. Ophthalmol. Vis. Sci.* **45** 2722–31
- Lee B, Litt M and Buchsbaum G 1992 Rheology of the vitreous body. Part I: viscoelasticity of human vitreous *Biorheology* **29** 521–33
- López-Cortés L F, Pastor-Ramos M T, Ruiz-Valderas R, Cordero E, Uceda-Montañés A, Claro-Cala C M and Lucero-Muñoz M J 2001 Intravitreal pharmacokinetics and retinal concentrations of ganciclovir and foscarnet after intravitreal administration in rabbits *Invest. Ophthalmol. Vis. Sci.* **42** 1024–48
- Lund-Andersen H 2003 *Adler's Physiology of the Eye (Vitreous)* 10th edn ed P L Kaufman and A Alm (St Louis, MO: Mosby) chapter 7 pp 291–316
- Moldow B, Sander B, Larsen M, Engler C, Li B, Rosenberg T and Lund-Andersen H 1998 The effect of acetazolamide on passive and active transport of fluorescein across the blood-retina barrier in retinitis pigmentosa complicated by macular oedema *Graefes Arch. Clin. Exp. Ophthalmol.* **236** 881–9
- Oliveri A, Stocchino A and Storace M 2011 Barriers to transport induced by periodic oscillations in a physical model of the human vitreous chamber *Phys. Rev. E* **83** 036311
- Picciorelli M, Bergamin O, Landau K, Boesiger P and Luechinger R 2012 Vitreous deformation during eye movement *NMR Biomed.* **25** 59–66
- Ranta V and Urtti A 2006 Transscleral drug delivery to the posterior eye: prospects of pharmacokinetic modeling *Adv. Drug Deliv. Rev.* **58** 1164–81

- Repetto R, Siggers J H and Stocchino A 2008 Steady streaming within a periodically rotating sphere *J. Fluid Mech.* **608** 71–80
- Repetto R, Siggers J H and Stocchino A 2010 Mathematical model of flow in the vitreous humor induced by saccadic eye rotations: effect of geometry *Biomech. Model Mech.* **9** 65–76
- Repetto R, Stocchino A and Cafferata C 2005 Experimental investigation of vitreous humour motion within a human eye model *Phys. Med. Biol.* **50** 4729–43
- Rittenhouse K D and Pollack G M 2000 Microdialysis and drug delivery to the eye *Adv. Drug Deliv. Rev.* **45** 229–41
- Rossi T, Querzoli G, Pasqualitto G, Iossa M, Placentino L, Repetto R, Stocchino A and Ripandelli G 2012 Ultrasound imaging velocimetry of the human vitreous *Exp. Eye Res.* **99** 98–104
- Siggers J H and Ethier C R 2012 Fluid mechanics of the eye *Annu. Rev. Fluid Mech.* **44** 347–72
- Stay M S, Xu J, Randolph T W and Barocas V H 2003 Computer simulation of convective and diffusive transport of controlled-release drugs in the vitreous humor *Pharm. Res.* **20** 96–102
- Stocchino A, Repetto R and Cafferata C 2007 Eye rotation induced dynamics of a Newtonian fluid within the vitreous cavity: the effect of the chamber shape *Phys. Med. Biol.* **52** 2021–34
- Stocchino A, Repetto R and Siggers J H 2010 Mixing processes in the vitreous chamber induced by eye rotations *Phys. Med. Biol.* **55** 453–67
- Tojo K and Isowaki A 2001 Pharmacokinetic model for in vivo/in vitro correlation of intravitreal drug delivery *Adv. Drug Deliv. Rev.* **52** 17–24
- Walton K A, Meyer C H, Harkrider C J, Cox T A and Toth C A 2002 Age-related changes in vitreous mobility as measured by video B scan ultrasound *Exp. Eye Res.* **74** 173–80
- Yasukawa T, Ogura Y, Tabata Y, Kimura H, Wiedemann P and Honda Y 2004 Drug delivery systems for vitreoretinal diseases *Prog. Retin. Eye Res.* **23** 253–81